RESEARCH ARTICLE

Global Change Biology **WILEY**

Optimality principles explaining divergent responses of alpine vegetation to environmental change

Ziqi Zhu[1] | Han Wang[1] | Sandy P. Harrison[1,2] | Iain Colin Prentice[1,3,4] | Shengchao Qiao[1] | Shen Tan[1]

[1]Department of Earth System Science, Ministry of Education Key Laboratory for Earth System Modelling, Institute for Global Change Studies, Tsinghua University, Beijing, China

[2]School of Archaeology, Geography and Environmental Sciences (SAGES), University of Reading, Reading, UK

[3]Georgina Mace Centre for the Living Planet, Department of Life Sciences, Imperial College London, Ascot, UK

[4]Department of Biological Sciences, Macquarie University, North Ryde, New South Wales, Australia

Correspondence

Han Wang, Department of Earth System Science, Ministry of Education Key Laboratory for Earth System Modelling, Institute for Global Change Studies, Tsinghua University, Beijing 100084, China.
Email: wang_han@mail.tsinghua.edu.cn

Abstract

Recent increases in vegetation greenness over much of the world reflect increasing CO_2 globally and warming in cold areas. However, the strength of the response to both CO_2 and warming in those areas appears to be declining for unclear reasons, contributing to large uncertainties in predicting how vegetation will respond to future global changes. Here, we investigated the changes of satellite-observed peak season absorbed photosynthetically active radiation (F_{max}) on the Tibetan Plateau between 1982 and 2016. Although climate trends are similar across the Plateau, we identified robust divergent responses (a greening of $0.31\pm0.14\%$ year^{-1} in drier regions and a browning of $0.12\pm0.08\%$ year^{-1} in wetter regions). Using an eco-evolutionary optimality (EEO) concept of plant acclimation/adaptation, we propose a parsimonious modelling framework that quantitatively explains these changes in terms of water and energy limitations. Our model captured the variations in F_{max} with a correlation coefficient (r) of .76 and a root mean squared error of .12 and predicted the divergent trends of greening ($0.32\pm0.19\%$ year^{-1}) and browning ($0.07\pm0.06\%$ year^{-1}). We also predicted the observed reduced sensitivities of F_{max} to precipitation and temperature. The model allows us to explain these changes: Enhanced growing season cumulative radiation has opposite effects on water use and energy uptake. Increased precipitation has an overwhelmingly positive effect in drier regions, whereas warming reduces F_{max} in wetter regions by increasing the cost of building and maintaining leaf area. Rising CO_2 stimulates vegetation growth by enhancing water-use efficiency, but its effect on photosynthesis saturates. The large decrease in the sensitivity of vegetation to climate reflects a shift from water to energy limitation. Our study demonstrates the potential of EEO approaches to reveal the mechanisms underlying recent trends in vegetation greenness and provides further insight into the response of alpine ecosystems to ongoing climate change.

KEYWORDS

climate change, CO_2 fertilization effect, eco-evolutionary optimality, sensitivity of vegetation to climate, Tibetan Plateau, vegetation cover prediction

1 | INTRODUCTION

Vegetation modulates the exchange of water, energy and carbon fluxes between the land and the atmosphere (Alkama & Cescatti, 2016; Forzieri et al., 2020). Satellite data reveal a global increase in vegetation cover in recent decades (Chen, Park, et al., 2019; Piao et al., 2020; Zhu et al., 2016) although this greening is not universal and some regions have experienced browning (Bonan & Doney, 2018; Myers-Smith et al., 2020). The observed greening trend has contributed to an enhancement of the land carbon sink (Chen, Ju, et al., 2019) and changes in biogeophysical properties, such as surface albedo and evapotranspiration (Forzieri et al., 2017), which together regulate surface temperature and reduce the rate of global warming (Alkama & Cescatti, 2016; Zeng et al., 2017).

Greening has been widely attributed to rising atmospheric CO_2 concentrations, climate change and other human activities (Chen, Park, et al., 2019; Piao et al., 2020; Zhu et al., 2016). Increases in atmospheric CO_2 concentration lead to an increase in photosynthetic uptake of CO_2 by leaves, enhance vegetation water-use efficiency and have had a positive impact on primary production and vegetation cover globally (Donohue et al., 2013; Ukkola et al., 2015). It is thought that warming has eased climatic constraints in colder regions, explaining the marked greening trend observed in high northern latitudes (Berner et al., 2020; Huang et al., 2017; Keenan & Riley, 2018). However, there is accumulating evidence that the thermal response of vegetation growth and carbon uptake has weakened in the past four decades (Keenan & Riley, 2018; Piao et al., 2014, 2017) for reasons that are still unclear, imposing large uncertainties on vegetation responses to future warming and vegetation feedbacks to the carbon cycle. Moreover, a browning trend has also been observed, particularly in some Arctic areas (Berner & Goetz, 2022; Myers-Smith et al., 2020; Phoenix & Bjerke, 2016). This further complicates understanding the response of vegetation cover to warming in cold regions.

The Tibetan Plateau, known as the 'third pole', has experienced rapid warming recently, with an increase of 0.35°C decade^{-1} since 1970 (Kuang & Jiao, 2016; Yang et al., 2014; Yao et al., 2019). This warming is markedly higher than the global mean warming, and comparable to that seen in the Arctic (Yao et al., 2019). The Tibetan Plateau is considered one of the most climatically sensitive and ecologically fragile regions of the world (Yao et al., 2012) and provides an opportunity to examine whether the response of vegetation to warming in cold regions is consistent between high and low latitudes. Despite the reports of a general greening across the Tibetan Plateau from remote sensing observations (Shen, Piao, Jeong, et al., 2015; Teng et al., 2021; Wang et al., 2019), site and subregional scale studies show a weakening of this trend and even browning responses to warming (Sun et al., 2016; Wang et al., 2022; Zhao et al., 2019)—challenging the idea that warming has a predominantly positive effect through extension of the growing season and enhancement of photosynthesis (Fu et al., 2014; Shen et al., 2016; Shen, Piao, Dorji, et al., 2015). Alternative hypotheses have been proposed to explain the responses of vegetation cover to warming

in the Tibetan Plateau (Liu et al., 2018; Yan et al., 2021). Changes in water availability, for example, may also be important in driving changes in vegetation productivity and phenology given the relatively arid climate of much of the region (Li et al., 2020; Shen et al., 2022; Wang et al., 2022). However, a unified and quantitative framework is still missing, and inevitably introduces uncertainties in the prediction of future vegetation changes and mitigation strategies in this fragile region.

Process-based global vegetation models predict vegetation cover as the result of plant carbon assimilation, respiration, allocation to leaves and turnover processes (Walker et al., 2014), and have been extensively used as a tool to attribute the changes in vegetation cover to diverse climate factors (Piao et al., 2020; Zhu et al., 2016). However, the complex model structures make it challenging to interpret the modelling results for an understanding of the underlying mechanisms. Moreover, these models generally overestimate vegetation cover for cold-limited ecosystems and report a stronger positive trend than observed over recent decades (Anav et al., 2013; Murray-Tortarolo et al., 2013). They also differ in the magnitude and sign of the projected change of vegetation greenness in response to elevated CO_2 concentration and warming (De Kauwe et al., 2014; Mahowald et al., 2016). These differing predictions arise because the way the modelled processes are parameterized and implemented for different plant functional types varies between models (Prentice et al., 2015). Intermodel differences reflect a lack of understanding of the control of these basic processes (De Kauwe et al., 2014). Recent work shows that eco-evolutionary optimality (EEO) approaches (Franklin et al., 2020; Harrison et al., 2021) can generate parsimonious predictions of key vegetation processes through the consideration of the necessary trade-offs that plants have to make in a given environment. EEO relies on natural selection eliminating uncompetitive plant strategies, assuming that plants acclimate or adapt to their environment on both shorter (days to months) eco-physiological timescales and on longer demographic and evolutionary timescales. An EEO approach to predicting vegetation cover, based on the idea of mass balance and maximum carbon profit, has been successfully applied to both natural vegetation (Yang et al., 2018) and crops (Qiao et al., 2020, 2021). A similar EEO approach can be used to explore the impacts of recent climate change on vegetation cover in a simple and transparent way.

In this study, we have used remotely sensed data to derive changes in peak vegetation cover between 1982 and 2016 and compare the observed trends to changes in climate and environmental factors. We developed a simple model that simulates primary production using an EEO-based approach to account for carbon allocation to leaves subject to constraints by water availability. We used this model to quantify the individual contributions of changes in precipitation, CO_2 concentration, radiation, vapour pressure deficit (VPD) and temperature to the observed trends in vegetation growth across the Tibetan Plateau and to examine the cause of the observed decline in the sensitivity of vegetation growth to climate change in recent decades. We show that both the observed vegetation changes on the Tibetan Plateau and the

observed changes in sensitivity to climate change can be explained by this simple model.

2 | MATERIALS AND METHODS

2.1 | Data

2.1.1 | Gridded climate data

We obtained daily climate data for the period 1982–2016 from the China Meteorological Forcing Dataset (CMFD) at a 0.1° spatial resolution (He et al., 2020). The meteorological variables from CMFD used in this study were specific humidity (q, kg/kg), air pressure (PRES, Pa), air temperature (TEMP, °C), precipitation (PREC, mm) and downward shortwave radiation (Srad, Wm^{-2}).

From the CMFD data, we calculated VPD (Pa) as the difference between saturated vapour pressure (e_s, Pa) and actual vapour pressure (e_a, Pa):

$$VPD = e_s - e_a = 611.0 \cdot e^{\left(\frac{17.27 TEMP}{TEMP+237.3}\right)} - \frac{PRES\, q}{0.378q + 0.622}. \quad (1)$$

Following Meek et al. (1984), we derived photosynthetic photon flux density (PPFD, $mol\,m^{-2}\,day^{-1}$) from solar radiation (Srad, Wm^{-2}):

$$PPFD = 60 \times 60 \times 24 \times 2.04 \times 10^{-6} \times Srad. \quad (2)$$

Precipitation was accumulated over the whole year. PPFD was accumulated over the growing season, while air temperature and VPD were averaged over the growing season. The thermal growing season was defined as the period when daily air temperature was continuously above 0°C. This definition of the thermal growing season is widely used in the literature (e.g. Dong et al., 2012; Xu et al., 2021) and has a physiological basis in the temperature requirement for plant growth after the cold season (Harrison et al., 2010). Nevertheless, the length of the growing season on the Tibetan Plateau defined in this way is longer than that derived from remote sensing products (e.g. Cheng et al., 2018; Ding et al., 2013; Wang et al., 2019). We therefore tested this definition using breakpoint regression, using the Strucchange package in R, of in situ measurements of gross primary production (GPP) at two grassland sites (CN-HaM, CN-Dan) and one shrubland site (CN-Ha2) from the Tibetan Plateau. This analysis (Figure S1) confirms that the shift from zero to positive GPP occurs at $0.32 \pm 0.24°C$, consistent with our choice of 0°C for the delineation of the thermal growing season. Given that moisture availability might influence the length of the growing season (Shen et al., 2022), we also tested whether including a soil moisture threshold improved the definition of the growing season at these sites using a soil moisture threshold equivalent to half the multiyear maximum soil water content. Including a soil moisture threshold had no impact at the CN-HaM and CN-Ha2 sites, and only produced a marginal improvement at the CN-Dan site (Figure S2). Furthermore, the temporal variability and trends were similar whether the growing season definition was based only on a thermal threshold or on both a thermal and moisture availability threshold (Figure S3). For simplicity, we therefore focus on the results based on using the thermal threshold only.

The annual time series of atmospheric CO_2 concentrations between 1982 and 2016 was obtained from the National Oceanic and Atmospheric Administration Earth System Research Laboratory (NOAA: https://www.esrl.noaa.gov/gmd/ccgg/trends/). We used ordinary least squares regression to calculate the trends of long-term annual total precipitation (PREC), growing season mean VPD, summer warmth index (SWI_0, yearly sum of monthly mean air temperatures above 0°C), growing season accumulated photosynthesis photon flux density (PPFD) and atmospheric CO_2 concentration (CO_2).

The CMFD was designed to provide a good representation of climate across China, but it is of interest to compare this with global data sets to see how well they reproduce the climate of the Tibetan Plateau. We therefore obtained daily climate data from the Climatic Research Unit-National Centers for Environmental Prediction (CRU-NCEP) data set, the data set used as climate forcing in the Trends in Net Land Carbon Exchange (TRENDY) Inter-model Comparison Project. The CRU-NCEP data set provides air temperature, precipitation, solar radiation, specific humidity and air pressure, with a spatial resolution of 0.5° (Viovy, 2018). We then compared the geographic patterns and temporal trends of climate variables derived from CRU-NCEP with those obtained using CMFD.

2.1.2 | Satellite data

In our primary analyses, we used the GIMMS third-generation fraction of absorbed photosynthetically active radiation fAPAR (fAPAR3g) data set (Zhu et al., 2013) as an index of vegetation cover. We use fAPAR in preference to other vegetation indices because it is the main driver of vegetation productivity (Myneni & Williams, 1994; Ryu et al., 2019) and has been widely employed to track the environmental limitations on vegetation (Forkel et al., 2015; Keenan & Riley, 2018). The extended version of the fAPAR3g data set covers the interval of 1982–2016, with a spatial resolution of 1/12° and a temporal resolution of 2 weeks and was resampled to 0.1° using bilinear interpolation to match the spatial resolution of the climate data.

We determined the annual maximum fAPAR (F_{max}) as the peak greenness, a proxy for the capacity of ecosystem primary production (Huang et al., 2018), at each 0.1° grid cell from the biweekly composites. The F_{max} at each geographic grid was then binned in climate space determined by the corresponding annual total precipitation and summer warmth index (SWI_0, an indicator of total annual heat load). The bin width was arbitrarily set to 50 mm for precipitation and 5°C month for SWI_0. By selecting F_{max} in the upper 90–95th percentile in each climate bin, we identified the grid cells with maximum fAPAR attainable for a given amount of

precipitation and temperature and the corresponding environmental variables for these grid cells. This binning procedure is designed to disentangle the respective effects of water and heat supply in limiting peak growth of vegetation and minimize the impact of nonclimatic influences on greenness on the analyses. Similar analyses were made in the climate space determined by annual total precipitation and potential gross primary production (A_0) with a bin width of 50 mm for precipitation and $100 \, \mathrm{g\, C\, m^{-2}\, year^{-1}}$ for A_0. Climate bins with <5 grid cells were not included in the analysis. Vegetation dynamics on the Tibetan Plateau were examined with F_{max} data in both geographic and climate space using ordinary least squares linear regression.

Changes in vegetation cover have been previously investigated using several different vegetation indices, derived from different satellite sensor systems and covering different periods of time. These studies also differ in whether they focus on changes in mean growing season or peak vegetation cover. To assess the robustness of our results, and to facilitate comparisons with other analyses of vegetation change on the Tibetan Plateau, we performed several additional analyses. Firstly, we analysed the impact of using mean growing season fAPAR (F_{mean}) rather than F_{max} on the trends. Secondly, we examined the strength of the trends in F_{max} and F_{mean} over different time periods, specifically focusing on changes before and after 2000 CE since some concerns have been raised about the reliability of GIMMS3g data before 2000 CE (Zhu et al., 2021). Finally, we conducted analyses of changes in alpine vegetation cover using 12 different remote sensing products (Table S1), including fAPAR, normalized difference vegetation index (NDVI), leaf area index (LAI), solar-induced fluorescence (SIF), enhanced vegetation index (EVI) and near-infrared reflectance vegetation index (NIRv) data from various data sources.

2.1.3 | Model validation data

We used in situ measurements of aboveground biomass as an additional validation of the model performance. Aboveground biomass measurements from 1689 sites on the Tibetan Plateau, compiled by Xia et al. (2018), were obtained from https://iopscience.iop.org/article/10.1088/1748-9326/aa9997/data. The measurements were all taken in July and early August, at the peak of vegetation growth on the Plateau, and are thus comparable to F_{max}. For comparability with the modelled F_{max}, which is driven by gridded climate data at 0.1° resolution, we averaged the aboveground biomass observations from individual sites within each 0.1° grid.

We also compared the simulated F_{max} with GPP from the PML-V2 model (Zhang et al., 2019), which uses MODIS LAI, albedo and emissivity products and climate data from the Global Land Data Assimilation System (GLDAS) as model inputs (Zhang et al., 2019). We computed the maximum annual GPP over the interval from 2003 to 2016 and converted these data to a spatial resolution of 0.1° using bilinear interpolation to match the spatial resolution of the simulated F_{max}.

2.2 | Log-sum-exp regression analysis

We applied log-sum-exp regression (Peng et al., 2021), which fits a continuous approximation to the minimum function, to explore the spatial dependence of vegetation cover on precipitation and SWI_0. A mixed-effect model in the 'nlmefit' function of MATLAB was used to perform this nonlinear regression with the 'year' as the random effect using the formula:

$$F_{max} = -\frac{1}{K} \ln\left(e^{-K \, kp \, PREC} + e^{-K \, kt \, SWI_0} + e^{-K \, f_{max}}\right), \qquad (3)$$

where maximum fAPAR (F_{max}) is the response variable; precipitation (PREC, mm) and summer warmth index (SWI_0, °C month) are the predictor variables; and K, kp, kt and f_{max} are parameters. The greater the value K, the closer this function is to the minimum function. Here, as recommended by Peng et al. (2021), K was set as a constant (10) while kp and kt fitted to observations are expressed as the change in F_{max} for a unit increase of precipitation and temperature, that is, the sensitivity of F_{max} to the precipitation and temperature in units of % mm^{-1} and % °C $month^{-1}$ respectively. f_{max}, set as a constant (.95), represents the maximum possible fraction of PAR that can be absorbed by a vegetation canopy (Turner et al., 2009; Yang et al., 2015).

2.3 | Modelling of maximum vegetation cover

We propose a theory to investigate the patterns of vegetation cover in space and time, by coupling the EEO and hydro-climatological rate limitation framework with a universal primary production model (P model: Stocker et al., 2020). The basic hypothesis is that peak vegetation cover is limited either by energy supply (in which case, allocation to leaves maximizes net energy profit) or by water supply (Figure 1).

2.3.1 | Prediction of gross primary production

The P model is a universal and extensively tested light use efficiency (LUE) model for GPP (Cai & Prentice, 2020; Stocker et al., 2020; Wang, Prentice, Davis, et al., 2017). It is based on the Farquhar–von Caemmerer–Berry (FvCB) model for biochemical processes (Farquhar et al., 1980) combined with EEO hypotheses (the least-cost and coordination hypotheses) to represent the adaptation of stomatal behaviour and photosynthetic capacities to environmental conditions (Prentice et al., 2014; Wang, Prentice, Keenan, et al., 2017). The least-cost hypothesis states that plants minimize the summed costs of maintaining carboxylation and transpiration capacity by regulating their leaf-internal CO_2 concentration (Prentice et al., 2014). The coordination hypothesis states that the carboxylation-limited rate (A_c) and electron transport-limited rate (A_J) of photosynthesis, the lesser of which determines the instantaneous photosynthetic rate, tend to equality (Wang, Prentice, Keenan, et al., 2017). Comparisons between predicted GPP and eddy covariance data show the P model
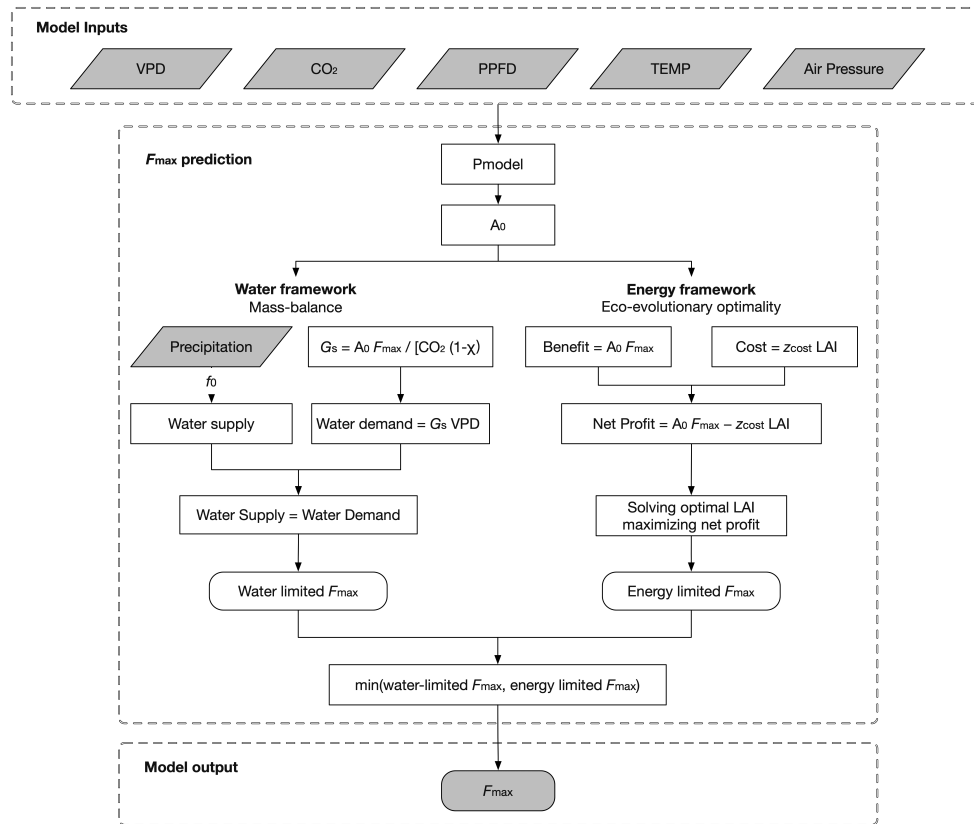
FIGURE 1 Flowchart of the prediction of the maximum fraction of absorbed photosynthetically active radiation (F_{max}). The model is based on the principle that the carbon allocation to leaves results from the maximization of net profit, subject to the constraint that water is available to allow optimal function of the leaves. Inputs of the model are growing season mean air pressure, growing season mean vapour pressure deficit (VPD), atmospheric carbon dioxide concentration (CO_2), growing season cumulative photosynthetic photon flux density (PPFD), growing season mean air temperature (TEMP) and annual total precipitation (precipitation). The output of the model is the annual maximum fAPAR. A_0, χ and G_s are the potential gross primary productivity; the ratio of leaf internal- to ambient-CO_2 concentration; and the stomatal conductance at canopy level respectively. A_0, χ and G_s are all predicted by the P model. f_0 is defined as the ratio of precipitation to transpiration and set at .41. z_{cost} represents the unit cost of constructing and maintaining leaves and is estimated as a function of air temperature and VPD.

performs as well as more complex models (Mengoli et al., 2021; Stocker et al., 2020).

Based on the P model, GPP (A) can be expressed as a product of fAPAR and potential gross primary production (A_0):

$$A = fAPAR\ A_0, \tag{4}$$

where A_0 is calculated as the product of LUE and PPFD:

$$A_0 = PPFD\ LUE. \tag{5}$$

In Equation (5):

$$LUE = \varphi_0 m \sqrt{1 - \left(\frac{c^*}{m}\right)^{\frac{2}{3}}}, \tag{6}$$

$$m = \frac{(c_i - \Gamma^*)}{(c_i + 2\Gamma^*)}, \tag{7}$$

$$\chi = \frac{c_i}{c_a} = \frac{\Gamma^*}{c_a} + \left(1 - \frac{\Gamma^*}{c_a}\right)\frac{\xi}{\left(\xi + \sqrt{VPD}\right)}, \tag{8}$$

$$\xi = \sqrt{\frac{\beta(K + \Gamma^*)}{1.6\eta^*}}, \tag{9}$$

where φ_0 is the intrinsic quantum yield of photosynthesis (mol CO_2 mol^{-1} photon). m reflects the impact of leaf-internal CO_2 on carbon assimilation, determined by the leaf-internal CO_2 partial pressure (c_i, Pa) and the CO_2 partial pressure compensation point (Γ^*, Pa); χ is the ratio of the leaf-internal to ambient CO_2 partial pressure (c_a, Pa); VPD (Pa); η^* the viscosity of water relative to its value at 25°C (dimensionless); K is the effective Michaelis–Menten coefficient of Rubisco (Pa) at a given temperature and atmospheric pressure. Two dimensionless constants ($c^* = .41$ and $\beta = 146$) are globally estimated from independent data.

2.3.2 | The EEO-based energy limitation

We propose that plants maximize net energy profit after the costs of constructing and supporting leaves are accounted for. fAPAR is

estimated from LAI (projected leaf area per unit ground area) by Beer's law (Monsi, 1953):

$$\text{fAPAR} = 1 - e^{-k\,\text{LAI}}, \tag{10}$$

where $k = 0.5$ is the extinction coefficient for photosynthetically active radiation. LAI (m^2 m^{-2}) is later solved as the optimal value that maximizes net carbon profit (P_n), which is assumed to be the difference between the carbon gain through assimilation (GPP) and the cost of constructing and maintaining leaves.

Net energy profit (P_n) is assumed to be equal to the difference between the energy gain through assimilation (GPP) and the cost of constructing and maintaining leaves:

$$P_n = \text{GPP} - z_{\text{cost}}\,\text{LAI}, \tag{11}$$

where z_{cost} (mol C m^{-2} year^{-1}) is the unit cost of constructing and maintaining leaves and depends on climate. It should be larger when the photosynthetic characteristics of the vegetation are affected by warming or increased aridity at relatively higher temperature, lower soil moisture, and/or higher VPD since more carbon needs to be allocated to root construction (Liu et al., 2018; Xu et al., 2012; Yan et al., 2021). Note that although both GPP and LAI have a large spatial variation, z_{cost} expresses the unit carbon cost requirements for the leaf, which varies much less across the Tibetan Plateau where grassland is the dominant vegetation coverage. Therefore, z_{cost} was assumed to be constant across the Tibetan Plateau each year.

Substituting Equation (4) into Equation (10), net profit can be expressed as:

$$P_n = A_0\left(1 - e^{-k\,\text{LAI}}\right) - z_{\text{cost}}\,\text{LAI}. \tag{12}$$

When the first derivative of Equation (12) is equal to zero, the turning point is a maximum, as the second derivative is always positive:

$$\frac{\partial P_n}{\partial \text{LAI}} = k\,A_0\,e^{-k\,\text{LAI}} - z_{\text{cost}} = 0. \tag{13}$$

Based on Equation (13), the optimal LAI can then be solved as:

$$\text{LAI} = \frac{1}{k}\ln\left(k\frac{A_0}{z_{\text{cost}}}\right). \tag{14}$$

Substituting Equation (10) into Equation (14) yields energy-limited fAPAR (fAPAR$_{\text{energy}}$):

$$\text{fAPAR}_{\text{energy}} = 1 - \frac{z_{\text{cost}}}{k A_0}. \tag{15}$$

The formula shows that in energy-limited conditions, peak vegetation cover should only be controlled by energy supply. The greater the A_0, the larger the fAPAR.

2.3.3 | The mass balance-based water limitation

The mass balance-based water limitation requires that transpiration (accompanied by carbon assimilation) should be matched by the water supply from precipitation (Qiao et al., 2020, 2021). We assume that vegetation makes use of a certain fraction (f_0) of precipitation to maintain its capacity for photosynthesis.

$$T = f_0\text{PREC}, \tag{16}$$

where T is the total transpiration in the growing season (mm year^{-1}), PREC is annual total precipitation (mm year^{-1}) and f_0 is the ratio of precipitation to transpiration (dimensionless), which depends on the partitioning of evapotranspiration (ET) and precipitation. To simplify the model, f_0 is set as a constant across the Tibetan Plateau.

The water demand of the vegetation can be estimated by Fick's Law (Tan et al., 2021):

$$T = 1.6\,G_s\,\text{VPD}, \tag{17}$$

where G_s is canopy conductance to CO_2.

Carbon assimilation, accompanied by transpiration, can be expressed as a function of canopy conductance (G_s), ambient CO_2 concentration (c_a) and the ratio of leaf-internal CO_2 (c_i) to c_a (χ) using Fick's law:

$$\text{GPP} = G_s\,c_a(1 - \chi). \tag{18}$$

Substituting Equation (18) into Equation (17), T can be calculated as:

$$T = \frac{1.6\,\text{fAPAR}\,A_0\,\text{VPD}}{c_a(1 - \chi)}. \tag{19}$$

Derived from Equations (16) and (19), based on the mass balance, water-limited vegetation cover (fAPAR$_{\text{water}}$) can be calculated as:

$$\text{fAPAR}_{\text{water}} = \frac{c_a(1 - \chi)\,f_0\,\text{PREC}}{1.6\,\text{VPD}\,A_0}. \tag{20}$$

2.3.4 | Parameter estimation

This framework posits that peak vegetation cover should be determined by the lesser of the water and energy-limited vegetation cover (Qiao et al., 2021). F_{max} can then be expressed as:

$$F_{\text{max}} = \min\left[1 - \frac{z_{\text{cost}}}{k A_0}, \frac{c_a(1 - \chi)\,f_0\,\text{PREC}}{1.6\,\text{VPD}\,A_0}, f_{\text{max}}\right]. \tag{21}$$

Here, f_{max} is set as a constant (.95) (Turner et al., 2009; Yang et al., 2015). It represents the maximum achievable fAPAR and is independent of other parameters. f_0 and z_{cost} are fitted by the observed fAPAR and climate data using log-sum-exp regression:

$$F_{max} = -\frac{1}{K}\ln\left[e^{-K\left(1-\frac{z_{cost}}{kA_0}\right)} + e^{-K\frac{c_a(1-\chi)\,f_0\,PREC}{1.6VPD\,A_0}} + e^{-K\,f_{max}}\right]. \quad (22)$$

We assume that z_{cost} can vary temporally but is spatially constant across the Tibetan Plateau. This simplification reflects the fact that the uneven distribution of samples along environmental gradients precludes an analysis of the spatial variability in z_{cost}. The fitted f_0 is quite conservative through time ($f_0 = 0.41 \pm 0.07$). However, the fitted z_{cost} shows a positive interannual trend (Figure S4), which is significantly related to temperature and VPD.

Maximum LAI is estimated from F_{max} based on Beer's law:

$$LAI_{max} = -\frac{1}{k}\ln(1-F_{max}). \quad (23)$$

2.4 | Diagnosing the contribution of environmental factors

We applied our model to diagnose the driving forces of greening and browning of the Tibetan Plateau. Six simulations with different inputs were used to assess the ability of the model to predict response patterns of vegetation cover to climate change and environmental factors. In the first experiment (PRE), all input variables varied over time. In the other five experiments (PREC, CO_2, PPFD, VPD, TEMP), the named input variable was held constant at its median value over the 35 years and the other variables were allowed to vary realistically. The difference between the PRE and each of the individual variable simulations provides a measure of the effect of single drivers. Similar analyses were used to diagnose the contribution of individual environmental factors to the trends in precipitation and temperature sensitivity.

3 | RESULTS

3.1 | Empirical analysis of the trends in vegetation greenness

The climate of the Tibetan Plateau changed significantly between 1982 and 2016. Annual total precipitation increased from 492 to 596 mm, implying an average increase of 3.1 mm year^{-1} (Figure S5a). The largest increases in the absolute amount of precipitation occurred in the driest areas, whereas the relatively small areas of the plateau with high precipitation experienced a slight decrease (Figures S6a, S7a and S8). Summer temperature, as measured by the accumulated temperature of the growing season (SWI$_0$), increased at a rate of 0.31°C month year^{-1} (Figure S5b). The thermal growing season became longer by 0.66 day year^{-1} (Figures S3 and S5c). As a result of the extended growing season, incident solar radiation as measured by accumulated PPFD during the growing season increased by 20.3 mol m^{-1} year^{-1} (Figure S5d). Although precipitation increased, atmospheric water demand as measured by VPD also increased by 0.0018 kPa year^{-1} (Figure S5e). The trends in SWI$_0$, PPFD and VPD are not spatially uniform, but they changed in the same direction across the whole of the region (Figures S6 and S7). Atmospheric CO_2 concentration, which is the principal driver of the changes in climate

but has additional effects on plant physiology and growth, increased from 341 ppm in 1982 to 404 ppm in 2016 (Figure S5f).

Although climate, radiation and CO_2 have changed in the same direction, the change in F_{max} across the Tibetan Plateau has not been uniform (Figure 2a). About half (53%) of the area has experienced greening and about half (47%) browning between 1982 and 2016. The greening trend is most pronounced in the northeast and northern part of the vegetated area, with a significant increase over 19% of the Plateau. Browning is more pronounced in the central and south-eastern parts of the Plateau and is significant over 15% of the area. These divergent trends in peak vegetation greenness are also seen in the GLASS product (Figure S9). In the climate space defined by annual total precipitation and SWI$_0$, we found that the rapid increase in peak vegetation occurred in areas with low annual precipitation (<500 mm) while browning occurred in areas with high precipitation (>500 mm) (Figure 2b).

The spatial patterns of greening and browning are largely robust to the use of F_{mean} instead of F_{max}. However, the trends in F_{mean} are weaker in both greening and browning regions (Figure S10) reflecting the fact that this measure is affected by changes in the length of the growing season whereas F_{max} is a more direct measure of the amount of carbon allocated to foliage to support vegetation growth. The greening and browning trends, as measured by F_{max}, are stronger during the interval 2001–2016 than during the interval from 1982 to 2000 (Figure S10). F_{mean} shows only limited evidence of browning during the earlier interval, when the general trends are weaker, although it does show significant greening in the south-western part of the plateau consistent with the results shown by F_{max}. The greening and browning trends during the recent interval (2001–2016) are consistent with trends shown by other vegetation indices, including GIMMS-derived maximum NDVI, SIF and MODIS-derived EVI and NIRv (Figure 2c). The consistency with SIF and NIRv is encouraging since these products are thought to be a good reflection of photosynthetic activity in non-forest and open vegetation (Badgley et al., 2017; Porcar-Castell et al., 2014). However, MODIS fAPAR and NDVI show a more extensive areas of greening and do not show the marked browning in the southern part of the plateau that is clearly identified in our analyses and the SIF products (Figure S8).

To confirm the robustness of the identified greening regions, we also applied the methodology proposed by Cortés et al. (2021) to account for temporal autocorrelation and the issue of multiple hypothesis testing, whereby we calculated the temporal autocorrelation at lag-1 for each grid cell (Figure S11) and then used a permutation test to detect greening regions across the Tibetan Plateau. This method is more conservative and so the area of significant greening and browning was reduced from 19% to 15% and from 11% to 9% respectively. Nevertheless, this reduction does not impact the identification of a greening trend in the northwestern part of the Plateau and a browning trend in the southeast (Figure S12). Cortés et al. (2021) also proposed the application of spatial clustering to reduce false-positive rates. However, as they recognized, this procedure makes it difficult to identify coherent trends in areas of complex topography, and thus, we did
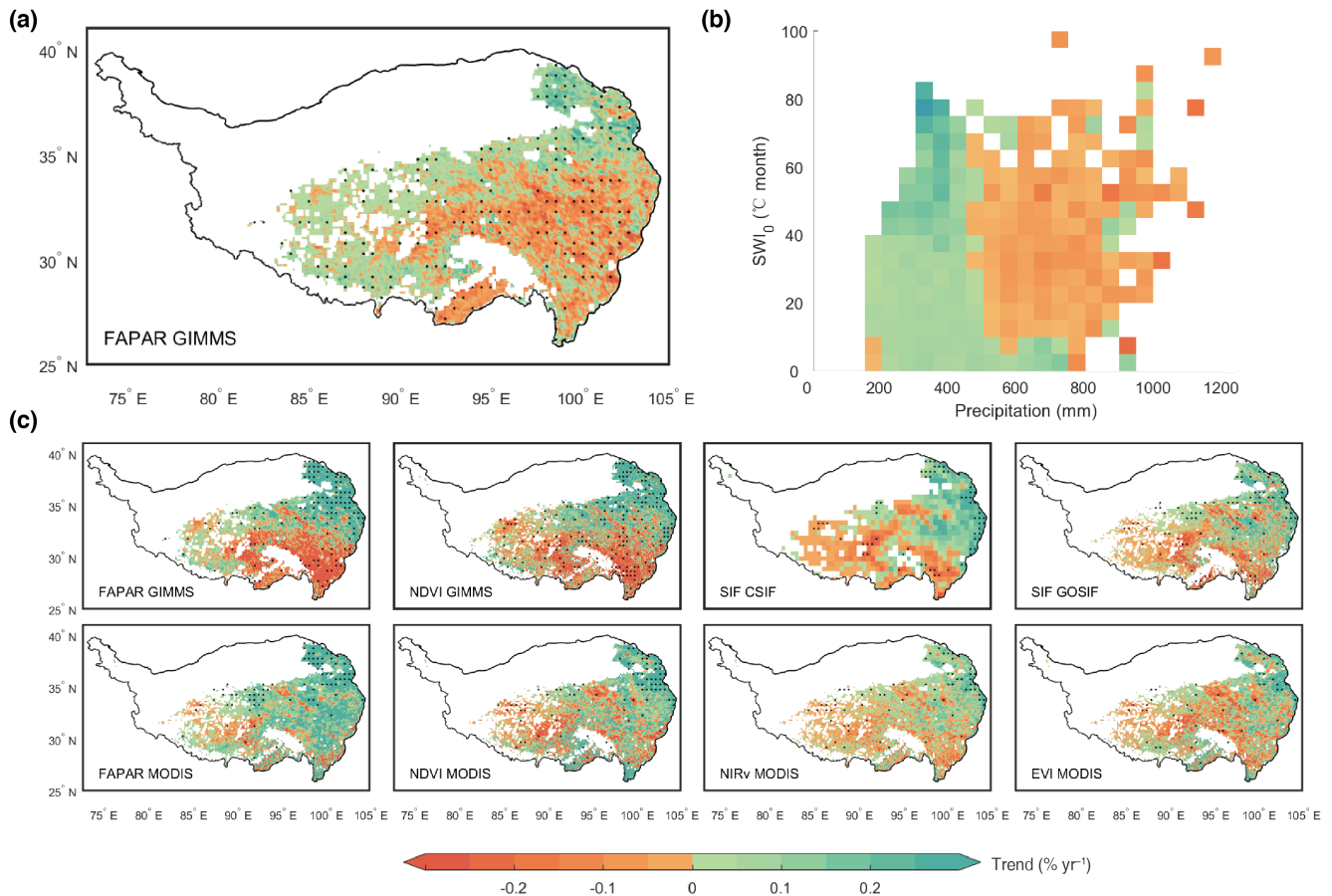
FIGURE 2 Divergent responses of alpine peak vegetation cover to environmental change. (a) Spatial distribution of the temporal trend of maximum fAPAR (F_{max}) over 1982–2016. (b) Trend of GIMMS F_{max} in the climate space of summer warmth index (SWI_0, a metric of growing season heat accumulation that is calculated as the sum of monthly temperatures above 0°C) and annual total precipitation (precipitation, a metric of water accumulation). The climate space is subdivided into different bins of equal intervals with bin widths arbitrarily set to 5°C month for SWI_0 and 50 mm for precipitation. Trends for each bin are calculated by averaging the subset of all pixels falling within that bin. Bins containing less than 5 pixels are not included. (c) Spatial distribution of the trend in alpine peak vegetation cover from multi-satellite proxies over 2001–2016 (depicted for GIMMS fAPAR3g and NDVI3g, CSIF, GOSIF, MODIS fAPAR, NDVI, NIRv and EVI) Grid cells labelled black dots indicate that the trends are statistically significant ($p < .05$).

not apply it here. Other indices for vegetation cover, including the mean and peak values of fAPAR during the growing season, LAI and NDVI, show similar spatial patterns to those identified using F_{max}, thus providing further confirmation that these trends are robust (Figure 2c). These divergent trends detected by multiple remote sensing-based products resulted in no significant change in the mean peak vegetation greenness across the Tibetan Plateau (Figure S12). In the climate space defined by annual total precipitation and SWI_0, we found that the rapid increase in peak vegetation occurred in areas with low annual precipitation (<500 mm) while browning occurred in areas with high precipitation (>500 mm) (Figure 2b).

F_{max} shows a strong relationship with both precipitation and temperature, with low values in drier and colder areas and high values in wetter and warmer areas. These two climate factors together explained 67% of the spatial variation in F_{max} (Figure 3a and Figure S14a). Log-sum-exp regression shows that F_{max} increased

approximately linearly with precipitation and temperature when water and heat supply are insufficient (i.e. in low precipitation and temperature conditions). F_{max} is even more closely related to precipitation and potential gross primary production (A_0) as calculated by the P model, with low F_{max} values in drier and low-energy supply areas and high values in wetter and high-energy supply areas (Figure 3b and Figure S14b). These two variables together account for around 75% of the spatial variation in F_{max}, reflecting the fact that potential gross primary production integrates the effects of SWI_0, PPFD and VPD on vegetation growth. The strong statistical relationship between climate and vegetation greenness is also seen in analyses using the GLASS product (Figure S15). This empirical analysis suggests that plant growth on the Tibetan Plateau may be limited by either water availability or energy availability, where water-limited areas are mainly located in the northwest of the Plateau and energy-limited areas in the centre and southeast (Figure S16).
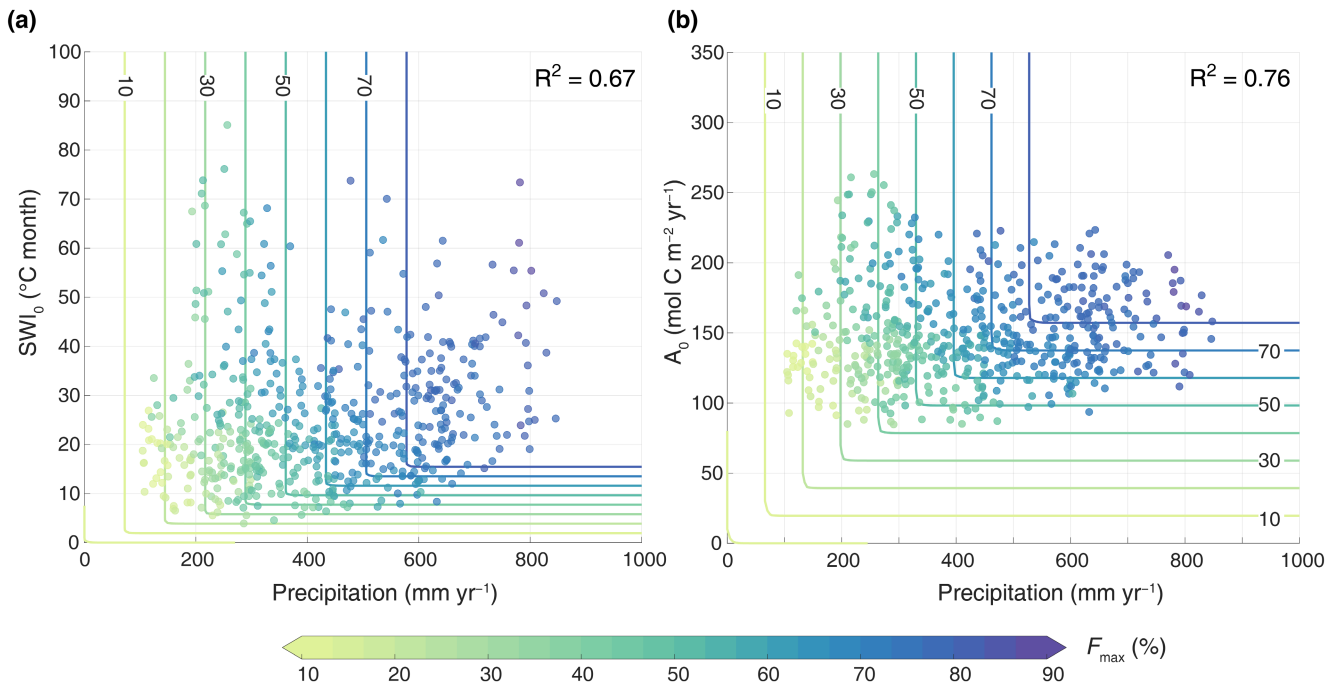
FIGURE 3 Relationship between peak vegetation growth and climate. (a) Relationship between F_{max} and total precipitation and summer warmth index (SWI_0) in 1982. (b) Relationship between F_{max} and total precipitation and potential gross primary production (A_0) in 1982. F_{max} selected in each 50 mm and 5°C month (50 mm and 100 g C m^{-2}) bin represents the maximum attainable vegetation cover for given annual precipitation and SWI_0 (A_0). Climate bins containing less than five grid cells are not included in these plots. Coloured lines represent the fitted contour of F_{max}, ranging from 0% to 80% with an interval of 10%.
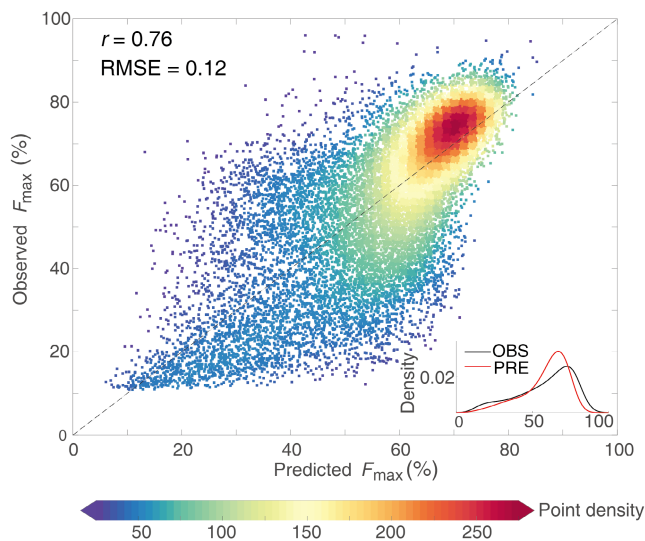

FIGURE 4 Comparison of estimated peak vegetation cover against observations. F_{max} data are collected in the climate space of annual total precipitation and summer warmth index (SWI_0) over 1982–2016. The density of points is represented by different colours. The black dashed line is the 1:1 line. The insert panel represents the probability density of predicted and observed F_{max}.

3.2 | Model validation

Our EEO-based model prediction of F_{max} is consistent with satellite observations (Figure 4), with a correlation coefficient (r) between predicted and observed GIMMS3g F_{max} of .76 and a root mean squared error (RMSE) of .12. Correlations of the spatial patterns for individual years ranged from .58 to .82 (Figure S17). Similar model performance is also shown for predictions of and GLASS F_{max} ($r = .79$ and RMSE = .11, Figure S18) and GIMMS3g LAI_{max} ($r = .75$ and RMSE = .69 m^2 m^{-2}, Figure S19). (Note that the larger RMSE for LAI_{max} reflects the different ranges for LAI_{max} and F_{max}.) The spatial comparison with MODIS-derived F_{max} and LAI_{max} also shows satisfactory agreement between observed and predicted values ($r = .67$ and RMSE = .12 m^2 m^{-2}, $r = .71$ and RMSE = .68 m^2 m^{-2}, Figure S20) without any recalibration of the model parameters. Comparison of predicted F_{max} with in situ measurements of aboveground biomass (Figures S21 and S22), resampled to the 0.1° resolution used for modelling, shows good agreement ($R^2 = .44$, $p < .001$). The model also shows good agreement ($r = .64$) with the simulated GPP derived from PML-V2 (Figure S23). Furthermore, the model correctly predicted the observed divergent trends in dry versus wet areas (Figure 5). The model predicted an increase in F_{max} of $0.32 \pm 0.19\%$
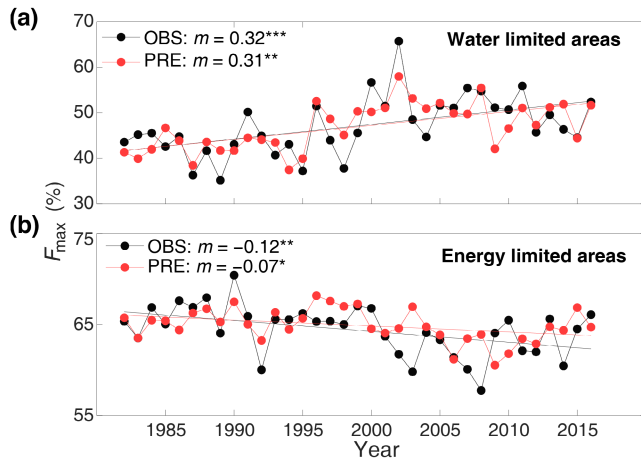
FIGURE 5 Trends in observed and predicted peak vegetation cover on the Tibetan Plateau. (a, b) Annual time series of observed GIMMS F_{max} (black line) and predicted F_{max} (red line) in water-limited areas (a) and energy-limited areas (b) over 1982–2016. F_{max} data are collected in the climate space of total precipitation and SWI_0. The solid lines show fitted linear regressions, with slope m (% year^{-1}) and p values indicated (*$p < .05$; **$p < .01$; ***$p < .001$).

year^{-1} in the water-limited areas, indistinguishable from the satellite-observed trend of $0.31 \pm 0.14\%$ year^{-1}. In energy-limited areas, the predicted F_{max} decreased by $0.07 \pm 0.06\%$ year^{-1}, close to (though somewhat smaller than) the observed decline of $0.12 \pm 0.08\%$ year^{-1}. The interannual variation in F_{max} is also well predicted by the model in both regions, though better in water-limited regions ($r = .75$) than energy-limited regions ($r = .45$).

3.3 | Diagnosis of the response of F_{max} to individual environmental variables

The factorial simulations show the relative contribution of different environmental factors to the observed trends in F_{max} (Figure 6). Increasing precipitation was the major driver of F_{max} trends in water-limited areas ($0.30 \pm 0.12\%$ year^{-1}) but was relatively unimportant in energy-limited areas ($0.010 \pm 0.004\%$ year^{-1}). Increasing CO_2 had a positive effect on vegetation cover overall, but the effect was larger in water-limited areas ($0.128 \pm 0.006\%$ year^{-1}) than in energy-limited areas ($0.077 \pm 0.003\%$ year^{-1}). Radiation had opposite effects in the two areas: increased radiation reduced vegetation cover in water-limited regions ($-0.100 \pm 0.035\%$ year^{-1}) but encouraged vegetation growth in energy-limited regions ($0.104 \pm 0.040\%$ year^{-1}). Increased VPD and warming had negative effects in both areas, but when compared with other environmental factors, the impact of VPD and warming was greater in energy-limited areas ($-0.106 \pm 0.043\%$ year^{-1}, $-0.132 \pm 0.031\%$ year^{-1} respectively) than water-limited areas ($-0.142 \pm 0.064\%$ year^{-1}, $-0.078 \pm 0.026\%$ year^{-1} respectively).

Our analyses show that the relationship between vegetation cover and climate has weakened over the past three decades (Figure 7). The model predictions indicate that the sensitivity of vegetation cover
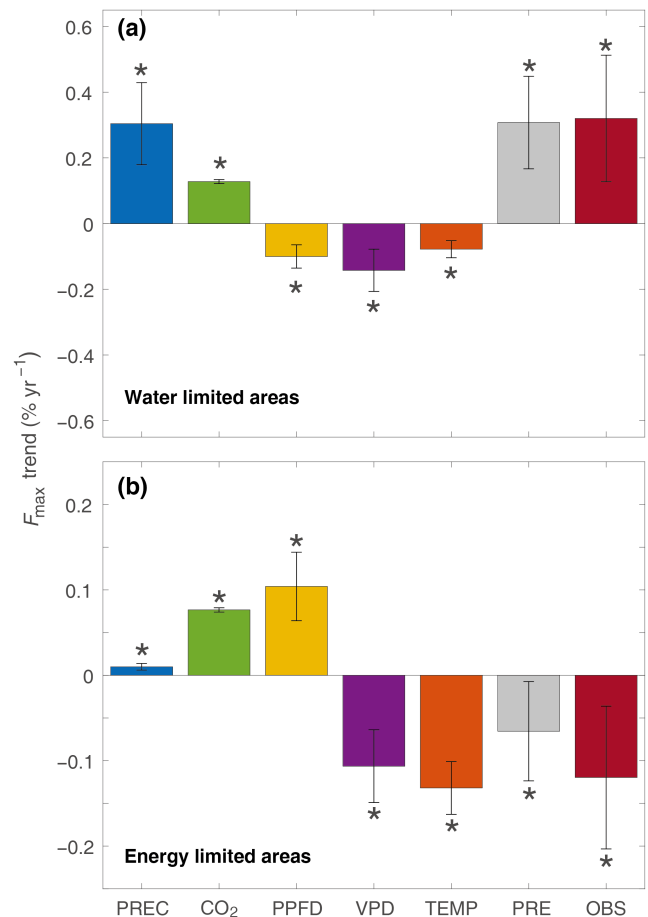

FIGURE 6 Attribution of trends in peak vegetation cover to various factors. (a, b) Trends in F_{max} derived from observation (OBS) and modelled trends driven by precipitation (PREC), rising CO_2 (CO_2), photosynthetic photon flux density (PPFD), vapour pressure deficit (VPD), temperature (TEMP) and all environmental factors (PRE) using the Mann–Kendall test in water-limited areas (a) and energy-limited areas (b). Error bars show the 95% confidence intervals of the regression. Statistically significant trends ($p < .05$) are marked with one asterisk.

to precipitation decreased by $13.6 \pm 3.9\%$ over the period between 1982 and 2016, while the sensitivity to temperature decreased by $36.9 \pm 15.6\%$. These declines in sensitivity are also seen in the satellite observations. The interannual variation in observed sensitivity is also captured by the model, though the performance of the model in predicting temperature sensitivity ($r = .89$) is better than predicting precipitation sensitivity ($r = .64$). Factorial simulations show that nearly half ($49.9 \pm 14.5\%$) of the decrease in temperature sensitivity results from increased temperature (Figure S24); the effect of increased temperature offsets the positive impacts of increased precipitation ($7.6 \pm 6.9\%$), elevated CO_2 ($3.6 \pm 0.7\%$) and increased PPFD ($21.6 \pm 10.0\%$) on vegetation growth. These factorial simulations also show that recent increases in CO_2 have a positive influence on the sensitivity of vegetation growth to precipitation. This somewhat counterintuitive result reflects the fact that although water-use efficiency increases with elevated CO_2 (Cheng et al., 2017; Keenan et al., 2013), the CO_2
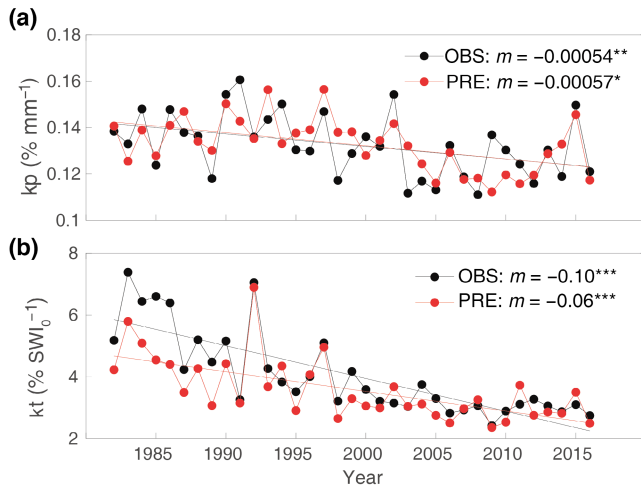
FIGURE 7 Weakened relationship between vegetation cover and climate. (a) Annual time series of observed (black line) and predicted (red line) sensitivity of vegetation cover to precipitation (kp) on the Tibetan Plateau over 1982–2016. (b) Annual time series of observed (black line) and predicted (red line) sensitivity of vegetation cover to temperature (kt) on the Tibetan Plateau over 1982–2016. Both the observed and predicted sensitivities of peak vegetation cover to climate are obtained from log-sum-exp regression in the climate space of precipitation and SWI_0. The solid lines show fitted linear regressions, with slope m (a, % mm^{-1} year^{-1}; b, % SWI_0^{-1} year^{-1}) and p values indicated ($*p < .05$; $**p < .01$; $***p < .001$).

induced enhancement of growth places high demands on water availability. The positive effect of CO_2 on the sensitivity of vegetation growth to increasing precipitation is offset by the negative influence of other variables. Specifically, the decreased sensitivity to precipitation is influenced both by changes in VPD and by changes in precipitation itself (Liu et al., 2021; Maurer et al., 2020), which contribute $7.8 \pm 2.2\%$ and $6.9 \pm 2.9\%$, respectively, to the decline in sensitivity. In water-limited environments (Figure S24b), plants respond to increases in VPD through stomatal closure (Ding et al., 2018; Yuan et al., 2019) and there is thus less transpiration and lower overall water demand. Under these conditions, increased precipitation does not translate into increased F_{max} because the water demand is already satisfied. The situation is different in energy-limited regions, where increased VPD inhibits photosynthesis and therefore directly reduces growth and the need for water. The declining sensitivity to precipitation reflects the fact that as precipitation increases, there is an overall shift from water limitation to energy limitation across the Tibetan Plateau, with water-limited areas shrinking and energy-limited areas expanding significantly (Figure S25). These changes mean there is a reduction in the water constraint on vegetation growth, such that vegetation growth becomes less sensitive to further increases in precipitation.

4 | DISCUSSION

We have developed an EEO-based approach to account for carbon allocation to leaves subject to constraints by water availability,

which requires calibration of only two parameters (f_0 and z_{cost}). We have shown that this parsimonious modelling framework accounts for changes in vegetation cover both at individual sites and regionally. Model predictions of F_{max} and LAI_{max} are consistent with observations, derived both from the GIMMS3g data from which the values of f_0 and z_{cost} were derived but also with MODIS-derived F_{max} and LAI_{max}. Comparisons of simulated F_{max} with in situ measurements of peak season above-ground biomass and GPP also show relatively good agreement; perfect agreement is not expected because these variables reflect not only variations in F_{max} but also variations in biomass per unit leaf area and its turnover rate, and vegetation light-use efficiency. Field measurements of F_{max} or LAI_{max} would be helpful for future model testing.

As a result of data constraints, specifically the risk of unevenly sampling environmental gradients, we have assumed that z_{cost} is spatially constant across the Tibetan Plateau but can vary through time. However, the fact that the temporal variability in z_{cost} is dependent on climate shows this is an oversimplification. While the satisfactory model performance indicates that this simplification has not had a large impact on our results overall, it would be informative to investigate the spatial and temporal variations in z_{cost} at a global scale. Given that this variability reflects changes in allocation to fine root construction and turnover (per unit leaf area), it should be possible to derive an EEO approach to predict z_{cost} as a function of environmental conditions.

We have identified divergent responses of maximum seasonal vegetation cover to recent observed climate changes in water-limited and energy-limited areas of the Tibetan Plateau. Previous studies of vegetation change, based on various MODIS-derived vegetation indices, have identified much stronger greening trends across the Plateau (Chen et al., 2020; Li et al., 2020; Shen, Piao, Jeong, et al., 2015; Wang et al., 2019) and not recognized this strong divergence, although Wei et al. (2022) have identified browning trends in the southern and eastern part of the Plateau between 1981 and 2015. Our analyses indicate that the regional extent, strength and significance of trends in vegetation cover are sensitive to whether the focus is on mean or peak growing season values, the sensor and vegetation indices used and the time period considered. The trends show up more strongly in peak growth than in the mean over the growing season, which reflects the fact that mean values are also influenced by changes in growing season length. The divergent trends are also stronger during recent decades than before 2000 CE, a finding consistent with that reported by Shen, Piao, Jeong, et al. (2015). While MODIS-derived fAPAR and LAI do not show the extent of browning shown by GIMMS3g-derived fAPAR and LAI, the divergent pattern is seen in the SIF and NIRv products from MODIS. Given that SIR and NIRv are considered to reflect vegetation structure and activity better than other indices (Bardgett et al., 2021; Li & Xiao, 2019), this suggests that our finding of divergent trends across the Plateau is robust. Nevertheless, it would be useful to have long-term field measurements at the ecosystem level, not only for investigating the differences in vegetation trends shown by different remote sensing products but also for monitoring the in situ vegetation changes (Piao et al., 2020).

Annual peak vegetation cover has been used to track environmental constraints on terrestrial ecosystem productivity in previous studies (Donohue et al., 2013; Huang et al., 2018; Keenan & Riley, 2018; Ukkola et al., 2015; Vicca, 2018). Most of these studies do not explicitly differentiate the responses in water-limited and energy-limited regions. However, Ukkola et al. (2015) found divergent trends in peak vegetation across Australia, with greening in water-limited areas and no significant change in carbon-limited areas. The divergent effects in water-limited and energy-limited regions of the Tibetan Plateau are a consequence of the fact that the long-term increase in growing season cumulative PPFD has opposite effects on water use and energy uptake (Figure 5 and Figure S26). In energy-limited areas, the observed lengthening of the growing season, and the consequent increase in cumulative radiation, stimulated photosynthesis (Ren et al., 2021). However, in arid or semiarid regions, increased PPFD increased potential productivity (A_0), resulting in increased water demand per unit leaf area and, since the water supply is limited, imposed a constraint on vegetation growth. This constraint has been partially offset by an increase in precipitation in water-limited areas, as also noted by Zhao et al. (2019), but changes in precipitation have had only a minor (albeit positive) effect on vegetation cover in energy-limited areas.

Increasing CO_2 concentrations have had a positive influence on peak vegetation cover in both energy- and water-limited areas, although the effect is almost twice as strong in water-limited areas. The same phenomenon has been observed in field experiments (Ainsworth & Long, 2005; Zhu et al., 2020). Increased water use efficiency with increasing atmospheric CO_2 concentration (Donohue et al., 2013; Keenan et al., 2013; Ukkola et al., 2015) reduces the water constraint in water-limited areas. In energy-limited areas, increased CO_2 concentration is expected to increase vegetation cover due to enhanced photosynthesis (Piao et al., 2020; Poorter et al., 2021). This enhancement, however, follows a saturating response curve of photosynthesis to CO_2, thus having a weaker effect than in water-limited areas. The negative impact of increasing VPD on vegetation growth in both energy- and water-limited areas of the Tibetan Plateau has also been observed in global analyses (Yuan et al., 2019). Increased VPD triggers stomatal closure, a mechanism for reducing water loss, leading to a decline in photosynthesis (Ding et al., 2018; Smith et al., 2020; Yuan et al., 2019).

We have shown that warming results in an apparent increase in the unit cost of constructing and maintaining leaves (z_{cost}). One interpretation of this is that warming leads to increases in below-ground carbon allocation. This is consistent with in situ observations and experimental evidence, from the Tibetan Plateau and some other regions (Liu et al., 2018; Xu et al., 2012; Yan et al., 2021). Liu et al. (2018), for example, have shown that warming leads to a shift towards deeper rooting and more below-ground carbon allocation in alpine grasslands on the Tibetan Plateau, allowing plants to acquire more water and nutrients. Xu et al. (2012) showed a similar shift in a long-term warming experiment in tallgrass prairie, although this response was modulated by water availability. Studies of the impact of warming in tundra vegetation show that increases in below-ground allocation in response to warming are not universal (Hollister & Flaherty, 2010; Wang et al., 2016); nevertheless, the observed decline in vegetation sensitivity to warming over the past three decades, noted in other studies (Keenan & Riley, 2018; Piao et al., 2014, 2017), may be a reflection of increased below-ground carbon allocation in regions where water supply is sufficient.

Our study confirms that the sensitivity of vegetation growth to increasing temperature has weakened in recent decades, as shown in other studies (Keenan & Riley, 2018; Piao et al., 2014, 2017). The magnitude of this decrease ($36.9 \pm 15.6\%$) on the Tibetan Plateau between 1982 and 2016 is similar to the value of 32.8% obtained from the analyses of the northern extratropics for the period between 1982 and 2012 (Keenan & Riley, 2018). In contrast to the findings of Keenan and Riley (2018) for the northern extratropics, this declining sensitivity does not translate into a reduction of the area that is energy limited on the Tibetan Plateau, which expanded by 11.8% over the period 1982–2016. This appears to be the result of the interplay between temperature and changes in other climate factors. The substantial increase in precipitation over the Plateau results in a decline in the area that is water limited but is insufficient to overcome the additional costs of constructing and maintaining leaves in energy-limited regions resulting from the increased radiation and atmospheric dryness. Several studies have shown that increasing precipitation has led to increased vegetation growth in dry regions (Liu et al., 2021; Maurer et al., 2020), and thus, a reduction in the area of water limitation as in the Tibetan Plateau. However, these studies have not explicitly examined changes in the overall sensitivity to increasing precipitation, which we have shown has also weakened in recent decades—albeit at a lower rate than the sensitivity to temperature. Understanding how this change in sensitivity to precipitation will affect the response to temperature will be important for understanding future changes in vegetation growth.

The regional extent, strength and significance of trends in vegetation cover are all sensitive to whether mean or peak growing season values are used, the indices used as a proxy for vegetation cover and the time period considered, as well as the statistical approaches used (Cortés et al., 2021). Here, we have used peak fAPAR as being the remotely sensed index closest to plant growth and have focused on peak growing season fAPAR values as likely to be most sensitive to environmental changes. We are able to reproduce the spatial patterns and trends in peak fAPAR using a simple and independently constructed EEO-based model of plant growth, which suggests that the reconstructed patterns over the Tibetan Plateau are realistic, and have diagnosed the impact of individual environmental factors on these trends. Process-based global vegetation models have been used to explore the causes of recent changes in vegetation cover (Piao et al., 2020; Winkler et al., 2021; Zhu et al., 2016). However, the global climate data sets used to drive these simulations represent the climate of the Tibetan Plateau poorly (see Figures S27 and S28) and this precludes any direct comparison of our results with existing process-based simulations. Nevertheless, EEO (Franklin

et al., 2020; Harrison et al., 2021) approaches have been shown to provide as good a representation of ecosystem processes as more complex global vegetation models (De Kauwe et al., 2015; Mengoli et al., 2021), and our analyses suggest that these approaches provide a useful alternative way of exploring the causes of recent vegetation changes.

5 | CONCLUSIONS

Despite having experienced similar climate trends over the last three decades, drier regions of the Tibetan Plateau have shown enhanced vegetation cover (greening) while wetter regions have shown decreased peak seasonal vegetation cover (browning). These divergent responses can be explained using a model that invokes the limitation of vegetation growth by energy or water. While recent increases in CO_2 have tended to increase vegetation cover in both energy- and water-limited regions, changes in temperature and atmospheric dryness (VPD) have impacted these regions differently. Warming has brought additional allocation costs, weakening the sensitivity of vegetation to temperature increases, particularly in energy-limited regions. This parsimonious modelling framework based on eco-evolutionary theory has thus succeeded in predicting maximum vegetation cover and its temporal trends, and the unexpected spatial divergence of these trends across the Tibetan Plateau. Our analysis demonstrates the potential of parsimonious EEO-based modelling to reveal the mechanisms underlying recent trends in vegetation cover and its sensitivity to climate change.

CONFLICT OF INTEREST

We declare we have no competing interests.

DATA AVAILABILITY STATEMENT

The GIMMS fAPAR3g and LAI3g data are available on request from R. Myneni (rmyneni@bu.edu; https://sites.bu.edu/cliveg/datacodes/). The CMFD climate data sets underlying the analysis are publicly available at Third Pole Environment Data Centre (http://data.tpdc.ac.cn/en/data/8028b944-daaa-4511-8769-965612652c49/). The CRU-NCEP climate data set can be obtained from https://rda.ucar.edu/datasets/ds314.3/. Carbon flux data from the CN-Ha2, CN-HaM, CN-Dan sites are available from FLUXNET (http://fluxnet.fluxdata.org/data/fluxnet2015-dataset/). Aboveground biomass measurements from 1689 sites on the Tibetan Plateau complied by Xia et al. (2018) can be downloaded at https://iopscience.iop.org/article/10.1088/1748-9326/aa9997/data.

ORCID

Ziqi Zhu https://orcid.org/0000-0003-0664-6032
Han Wang https://orcid.org/0000-0003-2482-1818
Sandy P. Harrison https://orcid.org/0000-0001-5687-1903
Iain Colin Prentice https://orcid.org/0000-0002-1296-6764
Shengchao Qiao https://orcid.org/0000-0002-4948-7062
Shen Tan https://orcid.org/0000-0001-5372-7850

REFERENCES

Ainsworth, E. A., & Long, S. P. (2005). What have we learned from 15 years of free-air CO_2 enrichment (FACE)? A meta-analytic review of the responses of photosynthesis, canopy properties and plant production to rising CO_2. *New Phytologist*, *165*(2), 351–371. https://doi.org/10.1111/j.1469-8137.2004.01224.x

Alkama, R., & Cescatti, A. (2016). Biophysical climate impacts of recent changes in global forest cover. *Science*, *351*(6273), 600–604. https://doi.org/10.1126/science.aac8083

Anav, A., Murray-Tortarolo, G., Friedlingstein, P., Sitch, S., Piao, S., & Zhu, Z. (2013). Evaluation of land surface models in reproducing satellite derived leaf area index over the high-latitude northern hemisphere. Part II: Earth system models. *Remote Sensing*, *5*(8), 3637–3661. https://doi.org/10.3390/rs5083637

Badgley, G., Field, C. B., & Berry, J. A. (2017). Canopy near-infrared reflectance and terrestrial photosynthesis. *Science Advances*, *3*(3). https://doi.org/10.1126/sciadv.1602244

Bardgett, R. D., Bullock, J. M., Lavorel, S., Manning, P., Schaffner, U., Ostle, N., Chomel, M., Durigan, G., Fry, E. L., Johnson, D., Lavallee, J. M., Le Provost, G., Luo, S., Png, K., Sankaran, M., Hou, X., Zhou, H., Ma, L., Ren, W., ... Shi, H. (2021). Combatting global grassland degradation. *Nature Reviews Earth & Environment*, *2*(10), 720–735. https://doi.org/10.1038/s43017-021-00207-2

Berner, L. T., & Goetz, S. J. (2022). Satellite observations document trends consistent with a boreal forest biome shift. *Global Change Biology*, *28*, 3275–3292. https://doi.org/10.1111/gcb.16121

Berner, L. T., Massey, R., Jantz, P., Forbes, B. C., Macias-Fauria, M., Myers-Smith, I., Kumpula, T., Gauthier, G., Andreu-Hayles, L., Gaglioti, B. V., Burns, P., Zetterberg, P., D'Arrigo, R., & Goetz, S. J. (2020). Summer warming explains widespread but not uniform greening in the Arctic tundra biome. *Nature Communications*, *11*(1), 4621. https://doi.org/10.1038/s41467-020-18479-5

Bonan, G. B., & Doney, S. C. (2018). Climate, ecosystems, and planetary futures: The challenge to predict life in Earth system models.

Science, *359*(6375), eaam8328. https://doi.org/10.1126/science.aam8328

Cai, W., & Prentice, I. C. (2020). Recent trends in gross primary production and their drivers: Analysis and modelling at flux-site and global scales. *Environmental Research Letters*, *15*(12), 124050. https://doi.org/10.1088/1748-9326/abc64e

Chen, C., Park, T., Wang, X., Piao, S., Xu, B., Chaturvedi, R. K., Fuchs, R., Brovkin, V., Ciais, P., Fensholt, R., Tommervik, H., Bala, G., Zhu, Z., Nemani, R. R., & Myneni, R. B. (2019). China and India lead in greening of the world through land-use management. *Nature Sustainability*, *2*, 122–129. https://doi.org/10.1038/s41893-019-0220-7

Chen, J. M., Ju, W., Ciais, P., Viovy, N., Liu, R., Liu, Y., & Lu, X. (2019). Vegetation structural change since 1981 significantly enhanced the terrestrial carbon sink. *Nature Communications*, *10*(1), 4259. https://doi.org/10.1038/s41467-019-12257-8

Chen, J., Yan, F., & Lu, Q. (2020). Spatiotemporal variation of vegetation on the Qinghai-Tibet plateau and the influence of climatic factors and human activities on vegetation trend (2000–2019). *Remote Sensing*, *12*(19), 3150. https://doi.org/10.3390/rs12193150

Cheng, M., Jin, J., Zhang, J., Jiang, H., & Wang, R. (2018). Effect of climate change on vegetation phenology of different land-cover types on the Tibetan Plateau. *International Journal of Remote Sensing*, *39*(2), 470–487. https://doi.org/10.1080/01431161.2017.1387308

Cheng, L., Zhang, L., Wang, Y. P., Canadell, J. G., Chiew, F. H. S., Beringer, J., Li, L., Miralles, D. G., Piao, S., & Zhang, Y. (2017). Recent increases in terrestrial carbon uptake at little cost to the water cycle. *Nature Communications*, *8*(1), 110. https://doi.org/10.1038/s41467-017-00114-5

Cortés, J., Mahecha, M. D., Reichstein, M., Myneni, R. B., Chen, C., & Brenning, A. (2021). Where are global vegetation greening and Browning trends significant? *Geophysical Research Letters*, *48*(6). https://doi.org/10.1029/2020gl091496

De Kauwe, M. G., Kala, J., Lin, Y. S., Pitman, A. J., Medlyn, B. E., Duursma, R. A., Abramowitz, G., Wang, Y. P., & Miralles, D. G. (2015). A test of an optimal stomatal conductance scheme within the CABLE land surface model. *Geoscientific Model Development*, *8*(2), 431–452. https://doi.org/10.5194/gmd-8-431-2015

De Kauwe, M. G., Medlyn, B. E., Zaehle, S., Walker, A. P., Dietze, M. C., Wang, Y. P., Luo, Y., Jain, A. K., El-Masri, B., Hickler, T., Warlind, D., Weng, E., Parton, W. J., Thornton, P. E., Wang, S., Prentice, I. C., Asao, S., Smith, B., McCarthy, H. R., … Norby, R. J. (2014). Where does the carbon go? A model-data intercomparison of vegetation carbon allocation and turnover processes at two temperate forest free-air CO_2 enrichment sites. *New Phytologist*, *203*(3), 883–899. https://doi.org/10.1111/nph.12847

Ding, J., Yang, T., Zhao, Y., Liu, D., Wang, X., Yao, Y., Peng, S., Wang, T., & Piao, S. (2018). Increasingly important role of atmospheric aridity on Tibetan alpine grasslands. *Geophysical Research Letters*, *45*(6), 2852–2859. https://doi.org/10.1002/2017gl076803

Ding, M., Zhang, Y., Sun, X., Liu, L., Wang, Z., & Bai, W. (2013). Spatiotemporal variation in alpine grassland phenology in the Qinghai-Tibetan Plateau from 1999 to 2009. *Chinese Science Bulletin*, *58*(3), 396–405. https://doi.org/10.1007/s11434-012-5407-5

Dong, M., Jiang, Y., Zheng, C., & Zhang, D. (2012). Trends in the thermal growing season throughout the Tibetan plateau during 1960–2009. *Agricultural and Forest Meteorology*, *166–167*, 201–206. https://doi.org/10.1016/j.agrformet.2012.07.013

Donohue, R. J., Roderick, M. L., McVicar, T. R., & Farquhar, G. D. (2013). Impact of CO_2 fertilization on maximum foliage cover across the globe's warm, arid environments. *Geophysical Research Letters*, *40*(12), 3031–3035. https://doi.org/10.1002/grl.50563

Farquhar, G. D., von Caemmerer, S., & Berry, J. A. (1980). A biochemical model of photosynthetic CO_2 assimilation in leaves of C3 species. *Planta*, *149*(1), 78–90. https://doi.org/10.1007/BF00386231

Forkel, M., Migliavacca, M., Thonicke, K., Reichstein, M., Schaphoff, S., Weber, U., & Carvalhais, N. (2015). Codominant water control on global interannual variability and trends in land surface phenology and greenness. *Global Change Biology*, *21*(9), 3414–3435. https://doi.org/10.1111/gcb.12950

Forzieri, G., Alkama, R., Miralles, D. G., & Cescatti, A. (2017). Satellites reveal contrasting responses of regional climate to the widespread greening of earth. *Science*, *356*(6343), 1180–1184. https://doi.org/10.1126/science.aal1727

Forzieri, G., Miralles, D. G., Ciais, P., Alkama, R., Ryu, Y., Duveiller, G., Zhang, K., Robertson, E., Kautz, M., Martens, B., Jiang, C., Arneth, A., Georgievski, G., Li, W., Ceccherini, G., Anthoni, P., Lawrence, P., Wiltshire, A., Pongratz, J., … Cescatti, A. (2020). Increased control of vegetation on global terrestrial energy fluxes. *Nature Climate Change*, *10*(4), 356–362. https://doi.org/10.1038/s41558-020-0717-0

Franklin, O., Harrison, S. P., Dewar, R., Farrior, C. E., Brannstrom, A., Dieckmann, U., Pietsch, S., Falster, D., Cramer, W., Loreau, M., Wang, H., Makela, A., Rebel, K. T., Meron, E., Schymanski, S. J., Rovenskaya, E., Stocker, B. D., Zaehle, S., Manzoni, S., … Prentice, I. C. (2020). Organizing principles for vegetation dynamics. *Nature Plants*, *6*(5), 444–453. https://doi.org/10.1038/s41477-020-0655-x

Fu, G., Shen, Z.-X., Sun, W., Zhong, Z.-M., Zhang, X.-Z., & Zhou, Y.-T. (2014). A meta-analysis of the effects of experimental warming on plant physiology and growth on the Tibetan plateau. *Journal of Plant Growth Regulation*, *34*(1), 57–65. https://doi.org/10.1007/s00344-014-9442-0

Harrison, S. P., Cramer, W., Franklin, O., Prentice, I. C., Wang, H., Brannstrom, A., de Boer, H., Dieckmann, U., Joshi, J., Keenan, T. F., Lavergne, A., Manzoni, S., Mengoli, G., Morfopoulos, C., Penuelas, J., Pietsch, S., Rebel, K. T., Ryu, Y., Smith, N. G., … Wright, I. J. (2021). Eco-evolutionary optimality as a means to improve vegetation and land-surface models. *New Phytologist*, *231*(6), 2125–2141. https://doi.org/10.1111/nph.17558

Harrison, S. P., Prentice, I. C., Barboni, D., Kohfeld, K. E., Ni, J., & Sutra, J.-P. (2010). Ecophysiological and bioclimatic foundations for a global plant functional classification. *Journal of Vegetation Science*, *21*(2), 300–317. https://doi.org/10.1111/j.1654-1103.2009.01144.x

He, J., Yang, K., Tang, W., Lu, H., Qin, J., Chen, Y., & Li, X. (2020). The first high-resolution meteorological forcing dataset for land process studies over China. *Scientific Data*, *7*(1), 25. https://doi.org/10.1038/s41597-020-0369-y

Hollister, R. D., & Flaherty, K. J. (2010). Above- and below-ground plant biomass response to experimental warming in northern Alaska. *Applied Vegetation Science*. https://doi.org/10.1111/j.1654-109X.2010.01079.x

Huang, K., Xia, J., Wang, Y., Ahlstrom, A., Chen, J., Cook, R. B., Cui, E., Fang, Y., Fisher, J. B., Huntzinger, D. N., Li, Z., Michalak, A. M., Qiao, Y., Schaefer, K., Schwalm, C., Wang, J., Wei, Y., Xu, X., Yan, L., … Luo, Y. (2018). Enhanced peak growth of global vegetation and its key mechanisms. *Nature Ecology & Evolution*, *2*(12), 1897–1905. https://doi.org/10.1038/s41559-018-0714-0

Huang, M., Piao, S., Janssens, I. A., Zhu, Z., Wang, T., Wu, D., Ciais, P., Myneni, R. B., Peaucelle, M., Peng, S., Yang, H., & Penuelas, J. (2017). Velocity of change in vegetation productivity over northern high latitudes. *Nature Ecology & Evolution*, *1*(11), 1649–1654. https://doi.org/10.1038/s41559-017-0328-y

Keenan, T. F., Hollinger, D. Y., Bohrer, G., Dragoni, D., Munger, J. W., Schmid, H. P., & Richardson, A. D. (2013). Increase in forest water-use efficiency as atmospheric carbon dioxide concentrations rise. *Nature*, *499*(7458), 324–327. https://doi.org/10.1038/nature12291

Keenan, T. F., & Riley, W. J. (2018). Greening of the land surface in the world's cold regions consistent with recent warming. *Nature Climate Change*, *8*, 825–828. https://doi.org/10.1038/s41558-018-0258-y

Kuang, X., & Jiao, J. J. (2016). Review on climate change on the Tibetan plateau during the last half century. *Journal of Geophysical Research:*

Atmospheres, *121*(8), 3979–4007. https://doi.org/10.1002/2015j d024728

Li, P., Hu, Z., & Liu, Y. (2020). Shift in the trend of browning in southwestern Tibetan plateau in the past two decades. *Agricultural and Forest Meteorology*, *287*, 107950. https://doi.org/10.1016/j.agrfo rmet.2020.107950

Li, X., & Xiao, J. (2019). A global, 0.05-degree product of solar-induced chlorophyll fluorescence Derived from OCO-2, MODIS, and reanalysis data. *Remote Sensing*, *11*(5). https://doi.org/10.3390/rs110 50517

Liu, D., Zhang, C., Ogaya, R., Fernandez-Martinez, M., Pugh, T. A. M., & Penuelas, J. (2021). Increasing climatic sensitivity of global grassland vegetation biomass and species diversity correlates with water availability. *New Phytologist*, *230*(5), 1761–1771. https://doi. org/10.1111/nph.17269

Liu, H., Mi, Z., Lin, L., Wang, Y., Zhang, Z., Zhang, F., Wang, H., Liu, L., Zhu, B., Cao, G., Zhao, X., Sanders, N. J., Classen, A. T., Reich, P. B., & He, J. S. (2018). Shifting plant species composition in response to climate change stabilizes grassland primary production. *Proceedings of the National Academy of Sciences of the United States of America*, *115*(16), 4051–4056. https://doi.org/10.1073/ pnas.1700299114

Mahowald, N., Lo, F., Zheng, Y., Harrison, L., Funk, C., Lombardozzi, D., & Goodale, C. (2016). Projections of leaf area index in earth system models. *Earth System Dynamics*, *7*(1), 211–229. https://doi. org/10.5194/esd-7-211-2016

Maurer, G. E., Hallmark, A. J., Brown, R. F., Sala, O. E., & Collins, S. L. (2020). Sensitivity of primary production to precipitation across the United States. *Ecology Letters*, *23*(3), 527–536. https://doi. org/10.1111/ele.13455

Meek, D. W., Hatfield, J. L., Howell, T. A., Idso, S. B., & Reginato, R. J. (1984). A generalized relationship between photosynthetically active radiation and solar radiation. *Agronomy Journal*, *76*(6), 939–945. https://doi.org/10.2134/agronj1984.00021962007600060018x

Mengoli, G., Agustí-Panareda, A., Boussetta, S., Harrison, S. P., Trotta, C., & Prentice, I. C. (2021). Ecosystem photosynthesis in landsurface models: A first-principles approach incorporating acclimation. *Journal of Advances in Modeling Earth Systems*, *14*. https://doi. org/10.1029/2021ms002767

Monsi, M. (1953). Uber den Lichtfaktor in den Pflanzen-gesellschaften und seine Bedeutung fur die Stoffproduktion. *Journal of Japanese Botany*, *14*, 22–52.

Murray-Tortarolo, G., Anav, A., Friedlingstein, P., Sitch, S., Piao, S., Zhu, Z., Poulter, B., Zaehle, S., Ahlström, A., Lomas, M., Levis, S., Viovy, N., & Zeng, N. (2013). Evaluation of land surface models in reproducing satellite-derived LAI over the high-latitude northern hemisphere. Part I: Uncoupled DGVMs. *Remote Sensing*, *5*(10), 4819–4838. https://doi.org/10.3390/rs5104819

Myers-Smith, I. H., Kerby, J. T., Phoenix, G. K., Bjerke, J. W., Epstein, H. E., Assmann, J. J., John, C., Andreu-Hayles, L., Angers-Blondin, S., Beck, P. S. A., Berner, L. T., Bhatt, U. S., Bjorkman, A. D., Blok, D., Bryn, A., Christiansen, C. T., Cornelissen, J. H. C., Cunliffe, A. M., Elmendorf, S. C., … Wipf, S. (2020). Complexity revealed in the greening of the Arctic. *Nature Climate Change*, *10*(2), 106–117. https://doi.org/10.1038/s41558-019-0688-1

Myneni, R. B., & Williams, D. L. (1994). On the relationship between FAPAR and NDVI. *Remote Sensing of Environment*, *49*(3), 200–211. https://doi.org/10.1016/0034-4257(94)90016-7

Peng, Y., Bloomfield, K. J., Cernusak, L. A., Domingues, T. F., & Prentice, I. C. (2021). Global climate and nutrient controls of photosynthetic capacity. *Communications Biology*, *4*(1), 462. https://doi. org/10.1038/s42003-021-01985-7

Phoenix, G. K., & Bjerke, J. W. (2016). Arctic browning: Extreme events and trends reversing arctic greening. *Global Change Biology*, *22*(9), 2960–2962. https://doi.org/10.1111/gcb.13261

Piao, S., Liu, Z., Wang, T., Peng, S., Ciais, P., Huang, M., Ahlstrom, A., Burkhart, J. F., Chevallier, F., Janssens, I. A., Jeong, S.-J., Lin, X., Mao, J., Miller, J., Mohammat, A., Myneni, R. B., Peñuelas, J., Shi, X., Stohl, A., … Tans, P. P. (2017). Weakening temperature control on the interannual variations of spring carbon uptake across northern lands. *Nature Climate Change*, *7*(5), 359–363. https://doi. org/10.1038/nclimate3277

Piao, S., Nan, H., Huntingford, C., Ciais, P., Friedlingstein, P., Sitch, S., Peng, S., Ahlstrom, A., Canadell, J. G., Cong, N., Levis, S., Levy, P. E., Liu, L., Lomas, M. R., Mao, J., Myneni, R. B., Peylin, P., Poulter, B., Shi, X., … Chen, A. (2014). Evidence for a weakening relationship between interannual temperature variability and northern vegetation activity. *Nature Communications*, *5*, 5018. https://doi.org/10.1038/ ncomms6018

Piao, S., Wang, X., Park, T., Chen, C., Lian, X., He, Y., Bjerke, J. W., Chen, A., Ciais, P., Tømmervik, H., Nemani, R. R., & Myneni, R. B. (2020). Characteristics, drivers and feedbacks of global greening. *Nature Reviews Earth & Environment*, *1*(1), 14–27. https://doi.org/10.1038/ s43017-019-0001-x

Poorter, H., Knopf, O., Wright, I. J., Temme, A. A., Hogewoning, S. W., Graf, A., Cernusak, L. A., & Pons, T. L. (2021). A meta-analysis of responses of C3 plants to atmospheric CO_2: Dose-response curves for 85 traits ranging from the molecular to the whole-plant level. *New Phytologist*, *233*, 1560–1596. https://doi.org/10.1111/nph.17802

Porcar-Castell, A., Tyystjärvi, E., Atherton, J., van der Tol, C., Flexas, J., Pfündel, E. E., Moreno, J., Frankenberg, C., & Berry, J. A. (2014). Linking chlorophyll a fluorescence to photosynthesis for remote sensing applications: Mechanisms and challenges. *Journal of Experimental Botany*, *65*(15), 4065–4095. https://doi.org/10.1093/ jxb/eru191

Prentice, I. C., Dong, N., Gleason, S. M., Maire, V., & Wright, I. J. (2014). Balancing the costs of carbon gain and water transport: Testing a new theoretical framework for plant functional ecology. *Ecology Letters*, *17*(1), 82–91. https://doi.org/10.1111/ele.12211

Prentice, I. C., Liang, X., Medlyn, B. E., & Wang, Y. P. (2015). Reliable, robust and realistic: The three R's of next-generation land-surface modelling. *Atmospheric Chemistry and Physics*, *15*(10), 5987–6005. https://doi.org/10.5194/acp-15-5987-2015

Qiao, S., Wang, H., Prentice, I. C., & Harrison, S. P. (2020). Extending a first-principles primary production model to predict wheat yields. *Agricultural and Forest Meteorology*, *287*, 107932. https://doi. org/10.1016/j.agrformet.2020.107932

Qiao, S., Wang, H., Prentice, I. C., & Harrison, S. P. (2021). Optimalitybased modelling of climate impacts on global potential wheat yield. *Environmental Research Letters*, *16*(11), 114013. https://doi. org/10.1088/1748-9326/ac2e38

Ren, Y., Yang, K., Wang, H., Zhao, L., Chen, Y., Zhou, X., & La, Z. (2021). The South Asia monsoon break romotes grass growth on the Tibetan plateau. *Journal of Geophysical Research: Biogeosciences*, *126*(3), e2020JG005951. https://doi.org/10.1029/2020jg005951

Ryu, Y., Berry, J. A., & Baldocchi, D. D. (2019). What is global photosynthesis? History, uncertainties and opportunities. *Remote Sensing of Environment*, *223*, 95–114. https://doi.org/10.1016/j. rse.2019.01.016

Shen, M., Piao, S., Chen, X., An, S., Fu, Y. H., Wang, S., Cong, N., & Janssens, I. A. (2016). Strong impacts of daily minimum temperature on the green-up date and summer greenness of the Tibetan plateau. *Global Change Biology*, *22*(9), 3057–3066. https://doi. org/10.1111/gcb.13301

Shen, M., Piao, S., Jeong, S. J., Zhou, L., Zeng, Z., Ciais, P., Chen, D., Huang, M., Jin, C. S., Li, L. Z., Li, Y., Myneni, R. B., Yang, K., Zhang, G., Zhang, Y., & Yao, T. (2015). Evaporative cooling over the Tibetan plateau induced by vegetation growth. *Proceedings of the National Academy of Sciences of the United States of America*, *112*(30), 9299–9304. https://doi.org/10.1073/pnas.1504418112

Shen, M., Wang, S., Jiang, N., Sun, J., Cao, R., Ling, X., Fang, B., Zhang, L., Zhang, L., Xu, X., Lv, W., Li, B., Sun, Q., Meng, F., Jiang, Y., Dorji, T., Fu, Y., Iler, A., Vitasse, Y., ... Fu, B. (2022). Plant phenology changes and drivers on the Qinghai–Tibetan plateau. *Nature Reviews Earth & Environment*, 1–19. https://doi.org/10.1038/s43017-022-00317-5

Shen, M. G., Piao, S. L., Dorji, T., Liu, Q., Cong, N., Chen, X. Q., An, S., Wang, S. P., Wang, T., & Zhang, G. X. (2015). Plant phenological responses to climate change on the Tibetan plateau: Research status and challenges. *National Science Review*, 2(4), 454–467. https://doi.org/10.1093/nsr/nwv058

Smith, M. N., Taylor, T. C., van Haren, J., Rosolem, R., Restrepo-Coupe, N., Adams, J., Wu, J., de Oliveira, R. C., da Silva, R., de Araujo, A. C., de Camargo, P. B., Huxman, T. E., & Saleska, S. R. (2020). Empirical evidence for resilience of tropical forest photosynthesis in a warmer world. *Nature Plants*, 6(10), 1225–1230. https://doi.org/10.1038/s41477-020-00780-2

Stocker, B. D., Wang, H., Smith, N. G., Harrison, S. P., Keenan, T. F., Sandoval, D., Davis, T., & Prentice, I. C. (2020). P-model v1.0: An optimality-based light use efficiency model for simulating ecosystem gross primary production. *Geoscientific Model Development*, 13(3), 1545–1581. https://doi.org/10.5194/gmd-13-1545-2020

Sun, J., Qin, X., & Yang, J. (2016). The response of vegetation dynamics of the different alpine grassland types to temperature and precipitation on the Tibetan plateau. *Environmental Monitoring and Assessment*, 188(1), 20. https://doi.org/10.1007/s10661-015-5014-4

Tan, S., Wang, H., Prentice, I. C., & Yang, K. (2021). Land-surface evapotranspiration derived from a first-principles primary production model. *Environmental Research Letters*, 16(10), 104047. https://doi.org/10.1088/1748-9326/ac29eb

Teng, H., Luo, Z., Chang, J., Shi, Z., Chen, S., Zhou, Y., Ciais, P., & Tian, H. (2021). Climate change-induced greening on the Tibetan plateau modulated by mountainous characteristics. *Environmental Research Letters*, 16(6). https://doi.org/10.1088/1748-9326/abfeeb

Turner, D. P., Ritts, W. D., Wharton, S., Thomas, C., Monson, R., Black, T. A., & Falk, M. (2009). Assessing FPAR source and parameter optimization scheme in application of a diagnostic carbon flux model. *Remote Sensing of Environment*, 113(7), 1529–1539. https://doi.org/10.1016/j.rse.2009.03.003

Ukkola, A. M., Prentice, I. C., Keenan, T. F., van Dijk, A. I. J. M., Viney, N. R., Myneni, R. B., & Bi, J. (2015). Reduced streamflow in water-stressed climates consistent with CO_2 effects on vegetation. *Nature Climate Change*, 6(1), 75–78. https://doi.org/10.1038/nclimate2831

Vicca, S. (2018). Global vegetation's CO_2 uptake. *Nature Ecology & Evolution*, 2(12), 1840–1841. https://doi.org/10.1038/s41559-018-0730-0

Viovy, N. (2018). *CRUNCEP Version 7—Atmospheric forcing data for the community land model.* https://doi.org/10.5065/PZ8F-F017

Walker, A. P., Hanson, P. J., De Kauwe, M. G., Medlyn, B. E., Zaehle, S., Asao, S., Dietze, M., Hickler, T., Huntingford, C., Iversen, C. M., Jain, A., Lomas, M., Luo, Y., McCarthy, H., Parton, W. J., Prentice, I. C., Thornton, P. E., Wang, S., Wang, Y.-P., ... Norby, R. J. (2014). Comprehensive ecosystem model-data synthesis using multiple data sets at two temperate forest free-air CO_2 enrichment experiments: Model performance at ambient CO_2 concentration. *Journal of Geophysical Research: Biogeosciences*, 119(5), 937–964. https://doi.org/10.1002/2013jg002553

Wang, H., Prentice, I. C., Davis, T. W., Keenan, T. F., Wright, I. J., & Peng, C. (2017). Photosynthetic responses to altitude: An explanation based on optimality principles. *New Phytologist*, 213(3), 976–982. https://doi.org/10.1111/nph.14332

Wang, H., Prentice, I. C., Keenan, T. F., Davis, T. W., Wright, I. J., Cornwell, W. K., Evans, B. J., & Peng, C. (2017). Towards a universal model for carbon dioxide uptake by plants. *Nature Plants*, 3(9), 734–741. https://doi.org/10.1038/s41477-017-0006-8

Wang, P., Heijmans, M. M. P. D., Mommer, L., van Ruijven, J., Maximov, T. C., & Berendse, F. (2016). Belowground plant biomass allocation in tundra ecosystems and its relationship with temperature. *Environmental Research Letters*, 11(5). https://doi.org/10.1088/1748-9326/11/5/055003

Wang, X., Wang, T., Liu, D., Zhang, T., Xu, J., Cui, G., Lv, G., & Huang, H. (2019). Multisatellite analyses of spatiotemporal variability in photosynthetic activity over the Tibetan plateau. *Journal of Geophysical Research: Biogeosciences*, 124(12), 3778–3797. https://doi.org/10.1029/2019jg005249

Wang, Y., Lv, W., Xue, K., Wang, S., Zhang, L., Hu, R., Zeng, H., Xu, X., Li, Y., Jiang, L., Hao, Y., Du, J., Sun, J., Dorji, T., Piao, S., Wang, C., Luo, C., Zhang, Z., Chang, X., ... Niu, H. (2022). Grassland changes and adaptive management on the Qinghai–Tibetan Plateau. *Nature Reviews Earth & Environment*, 1–16. https://doi.org/10.1038/s43017-022-00330-8

Wei, Y., Lu, H., Wang, J., Wang, X., & Sun, J. (2022). Dual influence of climate change and anthropogenic activities on the spatiotemporal vegetation dynamics over the Qinghai-Tibetan plateau from 1981 to 2015. *Earth's Future*, 10. https://doi.org/10.1029/2021ef002566

Winkler, A. J., Myneni, R. B., Hannart, A., Sitch, S., Haverd, V., Lombardozzi, D., Arora, V. K., Pongratz, J., Nabel, J. E. M. S., Goll, D. S., Kato, E., Tian, H., Almut, A., Friedlingstein, P., Atul, J., Zaehle, S., & Brovkin, V. (2021). Slowdown of the greening trend in natural vegetation with further rise in atmospheric CO_2. *Biogeosciences*, 18(17), 4985–5010. https://doi.org/10.5194/bg-18-4985-2021

Xia, J., Ma, M., Liang, T., Wu, C., Yang, Y., Zhang, L., Zhang, Y., & Yuan, W. (2018). Estimates of grassland biomass and turnover time on the Tibetan plateau. *Environmental Research Letters*, 13(1), 1–12. https://doi.org/10.1088/1748-9326/aa9997

Xu, H., Wang, H., Prentice, I. C., Harrison, S. P., Wang, G., & Sun, X. (2021). Predictability of leaf traits with climate and elevation: A case study in Gongga Mountain, China. *Tree Physiology*, 41(8), 1336–1352. https://doi.org/10.1093/treephys/tpab003

Xu, X., Niu, S., Sherry, R. A., Zhou, X., Zhou, J., & Luo, Y. (2012). Interannual variability in responses of belowground net primary productivity (NPP) and NPP partitioning to long-term warming and clipping in a tallgrass prairie. *Global Change Biology*, 18(5), 1648–1656. https://doi.org/10.1111/j.1365-2486.2012.02651.x

Yan, Y., Quan, Q., Meng, C., Wang, J., Tian, D., Wang, B., Zhang, R., & Niu, S. (2021). Varying soil respiration under long-term warming and clipping due to shifting carbon allocation toward below-ground. *Agricultural and Forest Meteorology*, 304–305, 108408. https://doi.org/10.1016/j.agrformet.2021.108408

Yang, J., Medlyn, B. E., De Kauwe, M. G., & Duursma, R. A. (2018). Applying the concept of ecohydrological equilibrium to predict steady state leaf area index. *Journal of Advances in Modeling Earth Systems*, 10(8), 1740–1758. https://doi.org/10.1029/2017ms001169

Yang, K., Wu, H., Qin, J., Lin, C., Tang, W., & Chen, Y. (2014). Recent climate changes over the Tibetan plateau and their impacts on energy and water cycle: A review. *Global and Planetary Change*, 112, 79–91. https://doi.org/10.1016/j.gloplacha.2013.12.001

Yang, Y., Donohue, R. J., McVicar, T. R., & Roderick, M. L. (2015). An analytical model for relating global terrestrial carbon assimilation with climate and surface conditions using a rate limitation framework. *Geophysical Research Letters*, 42(22), 9825–9835. https://doi.org/10.1002/2015gl066835

Yao, T., Thompson, L. G., Mosbrugger, V., Zhang, F., Ma, Y., Luo, T., Xu, B., Yang, X., Joswiak, D. R., Wang, W., Joswiak, M. E., Devkota, L. P., Tayal, S., Jilani, R., & Fayziev, R. (2012). Third pole environment (TPE). *Environment and Development*, 3, 52–64. https://doi.org/10.1016/j.envdev.2012.04.002

Yao, T., Xue, Y., Chen, D., Chen, F., Thompson, L., Cui, P., Koike, T., Lau, W. K. M., Lettenmaier, D., Mosbrugger, V., Zhang, R., Xu, B., Dozier, J., Gillespie, T., Gu, Y., Kang, S., Piao, S., Sugimoto, S., Ueno, K., ... Li, Q. (2019). Recent third Pole's rapid warming accompanies cryospheric

melt and water cycle intensification and interactions between monsoon and environment: Multidisciplinary approach with observation, modeling and analysis. *Bulletin of the American Meteorological Society*, *100*(3), 423–444. https://doi.org/10.1175/bams-d-17-0057.1

Yuan, W., Zheng, Y., Piao, S., Ciais, P., Lombardozzi, D., Wang, Y., Ryu, Y., Chen, G., Dong, W., Hu, Z., Jain, A. K., Jiang, C., Kato, E., Li, S., Lienert, S., Liu, S., Nabel, J., Qin, Z., Quine, T., … Yang, S. (2019). Increased atmospheric vapor pressure deficit reduces global vegetation growth. *Science Advances*, *5*(8), eaax1396. https://doi.org/10.1126/sciadv.aax1396

Zeng, Z., Piao, S., Li, L. Z. X., Zhou, L., Ciais, P., Wang, T., Li, Y., Lian, X., Wood, E. F., Friedlingstein, P., Mao, J., Estes, L. D., Myneni, R. B., Peng, S., Shi, X., Seneviratne, S. I., & Wang, Y. (2017). Climate mitigation from vegetation biophysical feedbacks during the past three decades. *Nature Climate Change*, *7*(6), 432–436. https://doi.org/10.1038/nclimate3299

Zhang, Y., Kong, D., Gan, R., Chiew, F. H. S., McVicar, T. R., Zhang, Q., & Yang, Y. (2019). Coupled estimation of 500 m and 8-day resolution global evapotranspiration and gross primary production in 2002–2017. *Remote Sensing of Environment*, *222*, 165–182. https://doi.org/10.1016/j.rse.2018.12.031

Zhao, J., Luo, T., Wei, H., Deng, Z., Li, X., Li, R., & Tang, Y. (2019). Increased precipitation offsets the negative effect of warming on plant biomass and ecosystem respiration in a Tibetan alpine steppe. *Agricultural and Forest Meteorology*, *279*, 107761. https://doi.org/10.1016/j.agrformet.2019.107761

Zhu, J., Zhang, Y., Yang, X., Chen, N., & Jiang, L. (2020). Synergistic effects of nitrogen and CO_2 enrichment on alpine grassland biomass and community structure. *New Phytologist*, *228*(4), 1283–1294. https://doi.org/10.1111/nph.16767

Zhu, Z., Bi, J., Pan, Y., Ganguly, S., Anav, A., Xu, L., Samanta, A., Piao, S., Nemani, R., & Myneni, R. (2013). Global data sets of vegetation leaf area index (LAI)3g and fraction of photosynthetically active radiation (FPAR)3g derived from global inventory modeling and mapping studies (GIMMS) normalized difference vegetation index (NDVI3g) for the period 1981 to 2011. *Remote Sensing*, *5*(2), 927–948. https://doi.org/10.3390/rs5020927

Zhu, Z., Piao, S., Myneni, R. B., Huang, M., Zeng, Z., Canadell, J. G., Ciais, P., Sitch, S., Friedlingstein, P., Arneth, A., Cao, C., Cheng, L., Kato, E., Koven, C., Li, Y., Lian, X., Liu, Y., Liu, R., Mao, J., … Zeng, N. (2016). Greening of the earth and its drivers. *Nature Climate Change*, *6*(8), 791–795. https://doi.org/10.1038/nclimate3004

Zhu, Z., Zeng, H., Myneni, R. B., Chen, C., Zhao, Q., Zha, J., Zhan, S., & MacLachlan, I. (2021). Comment on 'recent global decline of CO_2 fertilization effects on vegetation photosynthesis'. *Science*, *373*(6562), eabg5673. https://doi.org/10.1126/science.abg5673

SUPPORTING INFORMATION

Additional supporting information can be found online in the Supporting Information section at the end of this article.